A photomagnetic sponge: high-temperature light-induced ferrimagnet controlled by water sorption

Michał Magott,[a] Mateusz Reczyński,[a] Bartłomiej Gaweł,[b] Barbara Sieklucka,[a] Dawid Pinkowicz[a,*]

[a] Faculty of Chemistry, Jagiellonian University, Gronostajowa 2, 30-387 Kraków, Poland

[b] Department of Materials Science and Engineering, Norwegian University of Science and Technology (NTNU), 7491 Trondheim, Norway

Supporting Information Placeholder

ABSTRACT: 'Converting' light energy to magnetization is the attribute of molecule-based compounds called photomagnets and is inaccessible for conventional magnetic solids. The design and synthesis of such compounds, however, is a formidable challenge and only a few examples are known, all with rather low magnetic ordering temperatures well below the boiling point of liquid nitrogen. Herein, a cyanide-bridged coordination polymer $\{[Mn^{II}(imidazole)]_2[W^{IV}(CN)_8]\}_n$ exhibiting the highest light-induced magnetic ordering temperature ever observed and a magnetic hysteresis loop up to 90 K is reported. The photomagnetic effect results from the blue light excitation (450 nm) of the constituent octacyanotungstate(IV) moiety which then couples magnetically with manganese(II) resulting in light-induced ferrimagnetic ordering. The reported coordination framework shows also outstanding water sorption properties that are strongly correlated with the photomagnetic functionality. The photo-switching observed in the anhydrous state is completely quenched by the reversible capture of water with the fully hydrated phase becoming practically non-photomagnetic.

INTRODUCTION

Modern chemistry seeks new multifunctional materials showing complex physico-chemical properties.[1] In the same vein, molecular magnetism focuses on the construction of magnetic solids by design using molecules as building units. The target compounds are expected to show non-trivial magnetic properties strongly coupled with other functionalities[2] like photo-activity[3] or porosity.[4] Due to the basically unlimited number of combinations, it developed into a much broader and fascinating field of multifunctional molecular materials with magnetism being the main theme.

Molecular magnets that are responsive to visible light – photomagnets[2b] – constitute a special class of multifunctional magnetic materials where magnetization is controlled by photons. However, the preparation of building blocks showing inherent photomagnetic functionality is extremely challenging.[5] Photomagnetism is mainly studied in CN-bridged compounds with the Co^{II}-Fe^{III} [6] charge transfer pairs,[7] Fe^{II} spin cross-over complexes showing Light Induced Excited Spin State Trapping (LIESST)[8] and Co^{II}-dioxolene pairs.[9] 4*d* and 5*d* metal complexes are under-represented as LIESST candidates. Only recently, octacyanomolybdate(IV)[10] and octacyanotungstate(IV)[11] were demonstrated to show intrinsic LIESST-like behavior. In the case of CN-bridged Mn^{II}-$[W^{IV}(CN)_8]$-chains,[11] an enormous increase of the magnetization upon 436 nm irradiation was observed, yet the photo-induced long-range magnetic ordering or the magnetic hysteresis were never detected when the photomagnetic effect was based solely on the octacyanotungstate(IV). Herein, we present a three-dimensional (3-D) coordination polymer $\{[Mn^{II}(imidazole)]_2[W^{IV}(CN)_8]\}_n$ (**1**) showing light-induced long-range magnetic ordering above the boiling point of liquid nitrogen (LN_2) and a reversible hysteretic water capture at room temperature that controls the photomagnetic functionality. The light-induced magnetic ordering temperature of 93 K, magnetic hysteresis loop at 90 K and their control by water sorption are demonstrated for the first time.

RESULTS AND DISCUSSION

Structural studies

1 was obtained by the vacuum dehydration of $\{[Mn^{II}(imidazole)(H_2O)_2]_2[W^{IV}(CN)_8]\cdot 4H_2O\}_n$ (**1-8H$_2$O**), which was synthesized according to the modified procedure for Mo^{IV}-[12a] and Nb^{IV}-[12b] analogues. Single crystal X-ray diffraction studies of **1-8H$_2$O** (monoclinic, $P2_1/n$) revealed its three-dimensional (3-D) CN-bridged coordination skeleton of crossed-ladder topology. As depicted in **Figure 1a**, each W^{IV} forms six cyanide bridges towards six Mn^{II} centers, leaving two terminal cyanide ligands engaged in hydrogen bonds with crystallization water molecules and *aqua* ligands of the Mn^{II} ions (**Figure S1**). The $[W^{IV}(CN)_8]$ moiety attains intermediate geometry between the square antiprism and the dodecahedron (Continuous Shape Measure Analysis[13]; **Table S1**). As aforementioned, the vacuum dehydration of **1-8H$_2$O** (10^{-2} mbar, 24 h, RT) affords the water-free **1** (four crystallization and four coordination H_2O molecules removed). **1** was studied by means of the powder X-ray diffraction structural analysis (**Figure S2**, see Supporting Information for details; single crystals of **1-8H$_2$O** are crumbling in the process). The original crossed-ladder topology of **1-8H$_2$O** changes into square-grids-cross-linked-by-coordination-ladders in **1** (triclinic, $P\bar{1}$; **Figure 1b**) which is very similar to that reported for the Nb-analogue.[14] The complete removal of H_2O results in the formation of an additional W^{IV}-CN-Mn^{II} cyanide linkage and the change of the coordination number of Mn^{II} ions to five and four, respectively (**Figures 1c and 1d**). The tetracoordinate Mn^{II} resembles a distorted *pseudo*-vacant trigonal bipyramid where the "vacant" site is capped by an imidazole ring with the shortest Mn^{II}-$C_{imidazole}$ distance of 2.95 Å (**Figure S3**). This distance is significantly longer than that observed previously in the π-bonded stool-like geometry of the Mn^{II}-pyrrolide complex[15] (2.4-2.6 Å) which is the only other example of a stool-like Mn^{II} complex. The pentacoordinate Mn^{II} center, on the other hand, adopts a distorted trigonal bipyramidal

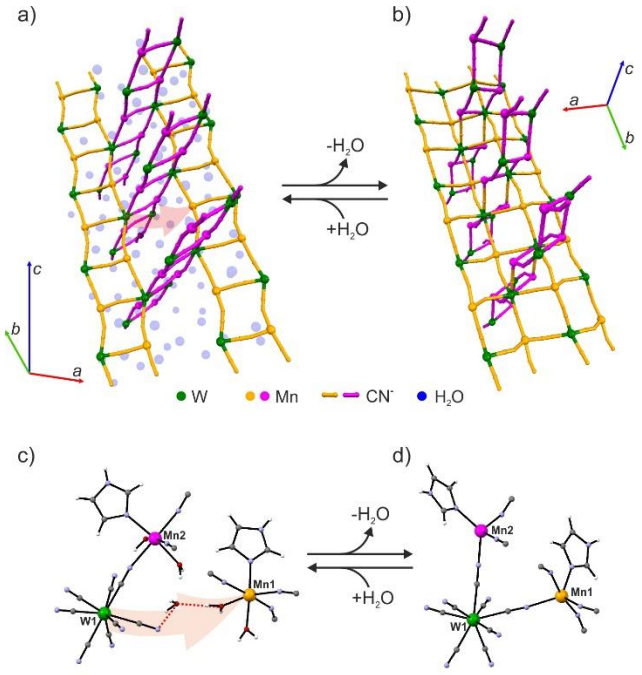

Figure 1. Strucutral diagrams showing the CN-bridged skeletons (a and b) and molecular fragments where CN-bridge formation occurs (c and d) in the prsitine **1-8H$_2$O** (a and c) and vacuum dehydrated **1** (b and d). Dehydration leads to the transformation of one set of ladder motifs into corrugated square-grids as a consequence of the CN-bridge formation (pink arrow in a and c) and the coordination number and geometry change of the Mn^{II} ions (C – gray, N – blue, O – red, H – white).

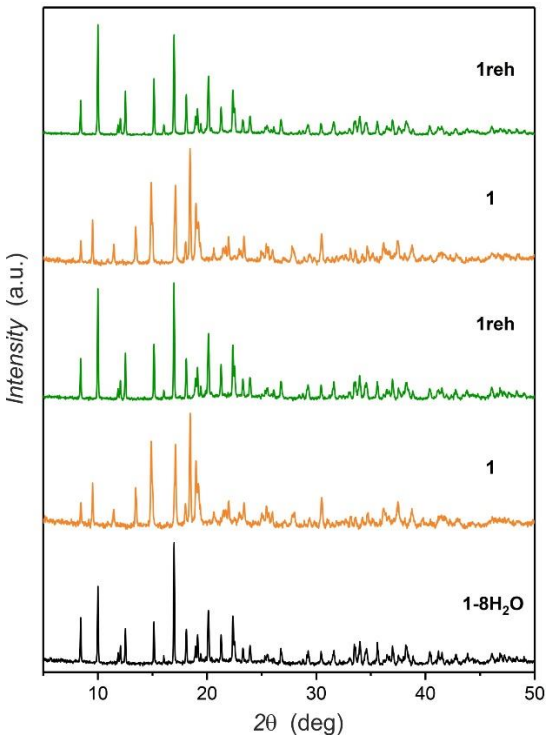

Figure 2. Experimental PXRD patterns for the pristine **1-8H$_2$O** (black), vacuum dehydrated **1** (orange) and rehydrated **1reh** (green) demonstrating the reversibility of the water sorption driven structural transformation. The dehydration-rehydration cycle was repeated twice.

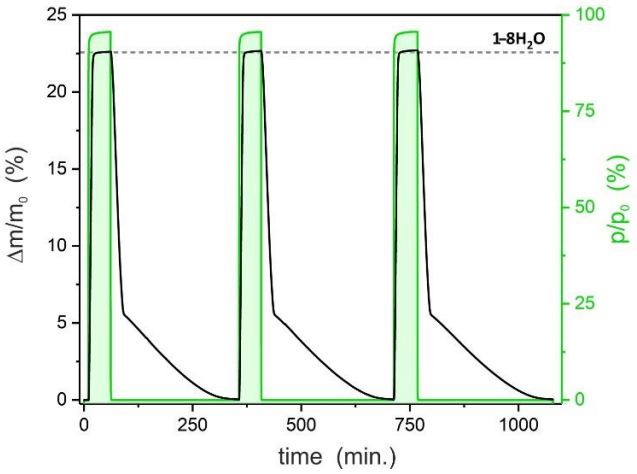

Figure 3. Relative mass change of **1** (black line) during cycling in the 0-95% relative humidity (RH) conditions at 298 K (green line). Dashed line shows the predicted mass for the fully hydrated form **1-8H$_2$O**.

geometry. The appearance of the tetracoordinate Mn^{II}-imidazole structural motif is accompanied by the formation of π-π stacks of four adjacent imidazole rings (**Figure S4**). Another structural change upon H_2O removal is the formation of an H-bond between the imidazole molecule and the remaining terminal cyanide ligand of the octacyanotungstate(IV)-moiety. All dehydration-induced structural changes leave no empty space in the crystal structure of the anhydrous phase. Yet, the dehydration process is reversible. The original structure and properties of **1-8H$_2$O** are completely restored by conditioning **1** at 95% relative humidity (RH) which leads to **1reh** $\{[Mn^{II}(imidazole)(H_2O)_2]_2[W^{IV}(CN)_8]\cdot 4H_2O\}_n$. **Figure 2** presents the experimental PXRD patterns for all three phases **1-8H$_2$O**, **1** and **1reh**.

Dynamic vapor sorption studies

The dehydration-rehydration cycles can be performed repeatedly with the full retention of the chemical identity of the compound (IR spectra in **Figure S5**). Dynamic vapor sorption studies at 298 K show that the complete rehydration of **1** is achieved within 10 minutes at 95% RH (**Figure 3**), with 22.6% relative mass increase perfectly matching the expected 22.57% corresponding to the absorption of eight water molecules per formula unit. **1** exhibits very good water sorption properties (**Figure S6**) of 0.19 g g^{-1} at P/P_0 = 0.3 as compared to typical water-harvesting systems under identical conditions: 0.30 g g^{-1} for MOF-801,[16a,b] 0.048 g g^{-1} for MCM-41,[17] 0.10 g g^{-1} for UiO-66,[18] 0.22 g g^{-1} for CAU-10,[19] 0.44 g g^{-1} for MOF-841,[16b] 0.9 g g^{-1} for Co_2Cl_2BTDD[16c] and 0.30 g g^{-1} for zeolite 13X[16b] (used for water adsorption chillers). Release of the adsorbed water occurs below 20% RH, with water content at P/P_0 = 0.1 equal to 0.060 g g^{-1}. Note, that other water sorption materials (i.e. molecular sieves or silica gels) might also be efficient at the investigated water pressure (P/P_0 = 0.3) but require higher regeneration temperature than MOFs or the reported compound. These properties make $\{[Mn^{II}(imidazole)]_2[W^{IV}(CN)_8]\}_n$ a very stable and convenient material for possible water harvesting applications at room temperature and very low humidity levels. Further studies in this vein are in progress.

Magnetic studies

The water-sorption-driven structural transformations of **1** have a significant impact on its magnetic properties. **1-8H$_2$O** and **1** show surprisingly different paramagnetic behavior. In the case of **1-8H$_2$O**, the χT value of 8.81 cm^3·K·mol^{-1} at 300 K is close to 8.75 cm^3·K·mol^{-1} expected for two octahedral Mn^{II} ions and remains

roughly constant down to 30 K. Below this temperature it decreases and reaches 5.94 $cm^3 \cdot K \cdot mol^{-1}$ at 1.8 K. The decrease is attributed to the weak antiferromagnetic interactions between the Mn^{II} centers (S_{Mn} = 5/2) through Mn^{II}-NC-W^{IV}-CN-Mn^{II} linkages (**Figure S7a**, green points). The paramagnetic behavior without any signs of magnetic anisotropy is also confirmed by the field dependence of the magnetization at 1.8 K (**Figure S8**, green points) and the successful simultaneous fitting of both $\chi T(T)$ and $M(H)$ using the following Hamiltonian (PHI software)[20]:

$$\hat{H} = -2J_{Mn\text{-}L\text{-}Mn} \cdot S_{Mn} \cdot S_{Mn} + \mu_B \cdot g_{Mn} \cdot S_{Mn} \cdot B + \mu_B \cdot g_{Mn} \cdot S_{Mn} \cdot B \quad \text{(Eq. 1)}$$

with the best fit parameters: g_{Mn} = 2.02(5) and J_{MnMn} = -0.07(1) cm^{-1} (assuming local $Mn^{II} \cdots Mn^{II}$ antiferromagnetic interactions only). The anhydrous phase **1** shows basically the same χT value as **1-8H₂O** (8.79 cm^3 K mol^{-1}) at room temperature as compared to the expected 8.75 cm^3 K mol^{-1} for two isotropic Mn^{II} ions. However, the $\chi T(T)$ exhibits a much stronger decrease than **1-8H₂O**, starting already at 90 K and reaching 2.60 cm^3 K mol^{-1} at 1.8 K (**Figure S7**, red points). The $M(H)$ dependence recorded at T = 2.0 K attains the maximum value of 9.5 Nβ at 7 T approaching the saturation of 10 Nβ expected for two isotropic Mn^{II} ions (**Figure S8**, red points). Simultaneous fitting of both $\chi T(T)$ and $M(H)$ (PHI software) using Eq. 1 reproduces well the former, but fails for the latter due to larger magnetic anisotropy that is not taken into account in the fitting (with the best fit parameters g_{Mn} = 2.02(5) and J_{MnMn} = -0.12(5) cm^{-1}). All these observations suggest that **1** is paramagnetic but cannot be considered a magnetically isotropic system. Noteworthy, the magnetic properties of **1reh** (after the 1st and the 2nd rehydration cycle) are identical to those of the pristine compound **1-8H₂O** (**Figures S7b** and **S8b**, green points). There is also basically no difference between the 1st and the 2nd dehydration cycle (**Figures S7b** and **S8b**, orange and red points), which confirms the "magnetic robustness" of **1-8H₂O** against repeated dehydration/rehydration.

Photomagnetic studies

Solid state electronic spectra of **1-8H₂O**, **1** and **1reh** are shown in **Figure S9**. The lowest energy bands at 440 nm for **1-8H₂O** and **1reh** (shoulder) and 450 nm for **1** correspond to the *d-d* transition of the octacyanotungstate(IV) anion. This spectral region is free of any other absorption bands (i.e. imidazole or the $[Mn^{II}$(imidazole)$]^{2+}$ moiety) making it a suitable target for photo-irradiation. The light-induced magnetic experiments were performed using a blue laser diode (λ = 450 nm, optical power at the sample 6-10 mW/cm^2). Surprisingly, **1-8H₂O** showed only an incremental magnetization change despite the constant 15 h irradiation at T = 10 K (**Figure 4**, green points). Only a negligible change of the temperature dependence of the magnetization $M(T)$ is observed (**Figure S10**). **1**, on the other hand, presents an unprecedented 15-fold increase of the χT at T = 10 K and H = 0.1 T (**Figure 4**, orange points; see also **Figure S11** in the SI that presents the mechanism of the photomagnetic effect in **1**). Moreover, the zero field-cooled (ZFC) and field-cooled (FC) magnetization curves measured at H = 20 Oe after irradiation bifurcate at 93 K (**Figure 5**), suggesting that the irradiation leads to a long-range magnetic ordering at the record critical temperature T_c = 93 K, well above the boiling point of liquid nitrogen (LN_2). This observation is fully supported by the opening of the magnetic hysteresis loops with M_r = 1.27 Nβ and H_c = 3400 Oe at 2.0 K (**Figure 6a**), M_r = 0.07 Nβ and H_c = 100 Oe at 77 K (**Figure 6b**) and M_r = 0.007 Nβ and H_c = 25 Oe at 90 K (**Figure 6c**) constituting the first system with the photo-induced magnetic hysteresis loop above the LN_2 boiling point (**Table S2**). The broad maximum in the ZFC curve around 25 K (Figure 5) indicate that some parts of the sample (the inside) with weaker illumination might show spin glass behavior below 60 K. This, however, does not influence the long-range magnetic ordering of the surface layers, the T_c of 93 K or the hysteresis loops at 77 and 90 K.

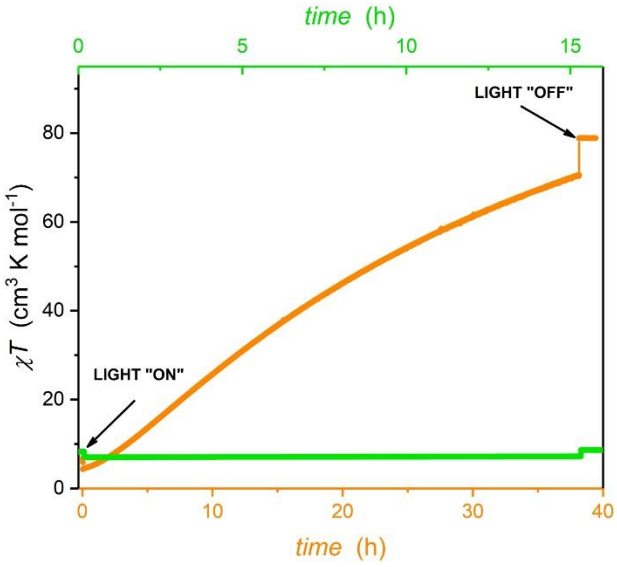

Figure 4. χT vs. time dependence recorded for **1-8H₂O** (green) and **1** (orange) at T = 10 K and H = 0.1 T during the irradiation experiment using a blue laser diode λ = 450 nm. The initial decrease of the χT product after turning the light on is a heating effect of the laser light. The increase after switching the light off is the reverse effect due to the sample cooling.

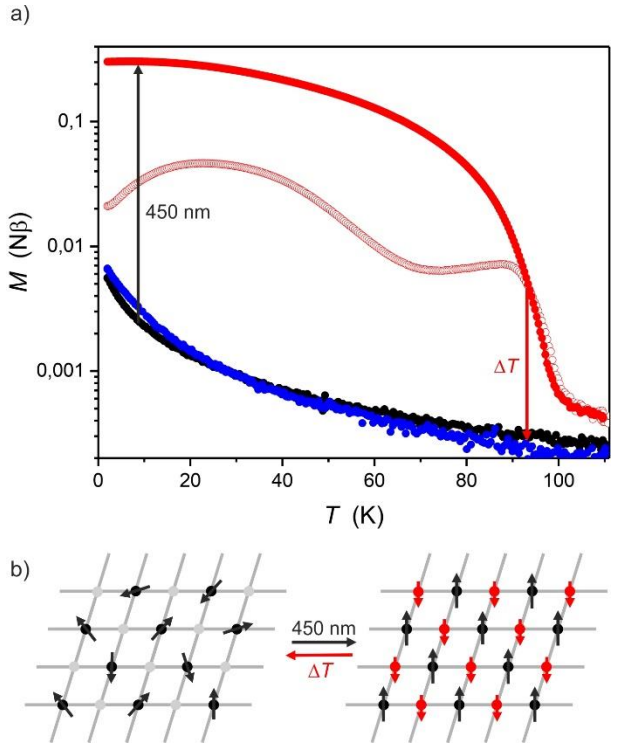

Figure 5. $M(T)$ at H = 0.002 T (3 $K \cdot min^{-1}$ temperature ramp) for compound **1** during the photo-irradiation experiment (a) and an illustration of the photo-conversion of the paramagnetic state into a magnetically ordered meta-stable ordered (b). The paramagnetic state (before irradiation – black points) undergoes a photo-induced transformation into a magnetically ordered state upon 450 nm light irradiation (red points – FC, red circles – ZFC), which after heating to 300 K fully relaxes to the original paramagnetic ground state (blue points).

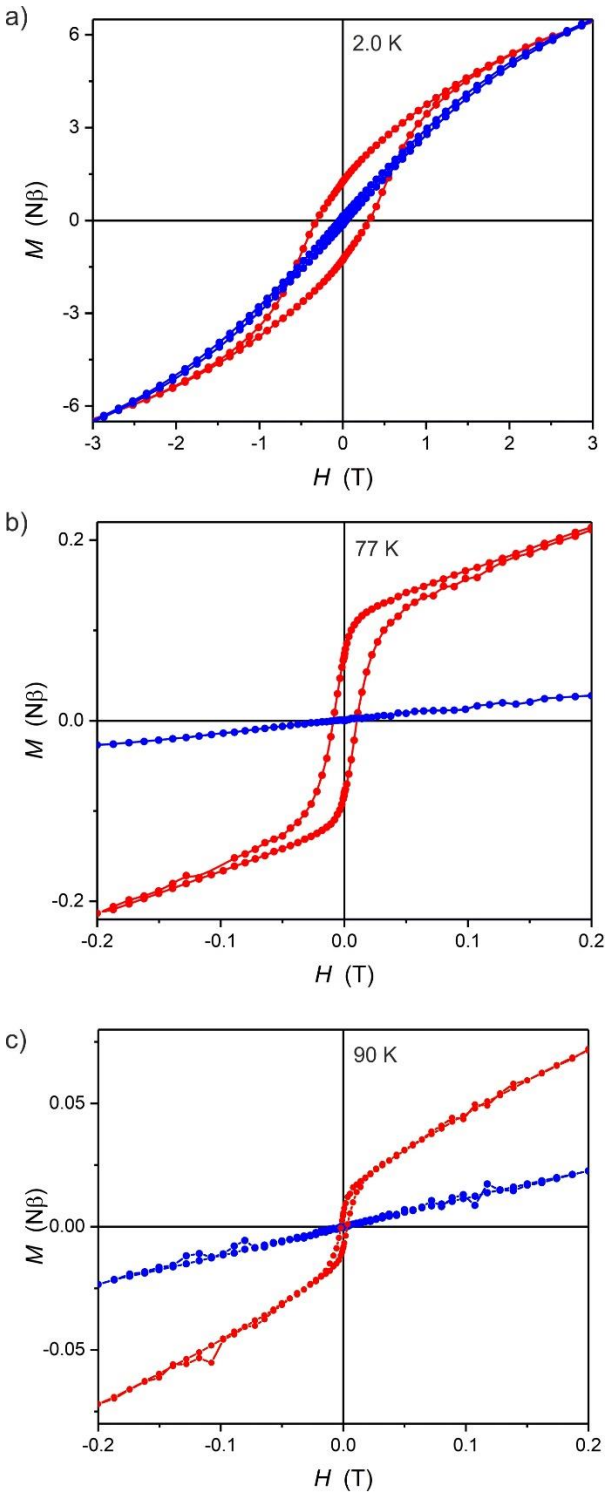

Figure 6. *M*(*H*) magnetic hysteresis loops measured at 2.0 (a), 77 (b) and 90 K (c) after 450 nm light irradiation (red points) and after thermal relaxation at 300 K (blue points).

The photomagnetic behavior of **1** is caused by the light-induced excited spin state trapping of the $[W^{IV}(CN)_8]^{4-}$ (W^{IV}_{HS}; $S = 1$) postulated before[10,11] and the consecutive activation of the W^{IV}_{HS}-CN-Mn^{II} magnetic interaction pathways through the extensive cyanide skeleton of **1**. The character of the magnetic interactions between the high-spin octacyanotungstate(IV) and the manganese(II) can be deduced from the analysis of the *M*(*H*) dependences recorded at *T* = 2.0 K. The *M*(*H*) curve after irradiation shows a significantly faster increase below 3 T compared to that before irradiation and reaches significantly lower value at 7 T - only 8.3 Nβ vs. 9.5 Nβ before irradiation (**Figure S12**). Such a behavior can be explained assuming antiferromagnetic interactions between Mn^{II} ($S = 5/2$) and the photo-induced high spin W^{IV}_{HS} ($S = 1$) resulting in the long-range ferrimagnetic ordering (see **Figure S13** in the Supporting Information for a detailed explanation of this deduction). Similar antiferromagnetic interactions were observed and described for photomagnetic $\{[Mn^{II}(bpy)_2][Mn^{II}(bpy)(H_2O)_2][W^{IV}(CN)_8]\cdot 5H_2O\}_n$ chains[11] although the long-range ordered state was not observed in that case.

The light-induced effect can be reversed by heating **1** to 300 K (compare the *M*(*T*) dependences recorded before irradiation and after thermal relaxation shown in **Figure 5**). **Figure S14** presents $\chi T(T)$ curves at 0.1 T measured before and after irradiation in the heating mode, which coincide around 200 K constituting the relaxation temperature for this system. Above 200 K the photo-excited W^{IV}_{HS} ions relax to the non-magnetic ground state (initial state). The slight differences in the *M*(*H*) curves before irradiation and after thermal relaxation (black and blue points in **Figure S12**) indicate a minimal damage of the sample. The slight decomposition is also visible in the IR spectra discussed in the Supporting Information (**Figures S15-S17**). The irreversibility might be caused by a photo-induced dissociation of the W-CN bond.[21] A mechanism of the photomagnetic effect based on the ligand photo-dissociation was postulated for the Cu^{II}-$[Mo^{IV}(CN)_8]$ molecules.[22] The possible photo-induced metastable state $[W^{IV}(CN)_7\cdot CN]$ is supported by the recent report of the heptacyanotungstate(IV) complex anion, which is paramagnetic ($S = 1$).[23] The IR spectra recorded during the sample irradiation at 90 K present limited evidence for the aforementioned structural reorganization as the key for understanding the photomagnetism in **1** (**Figure S17**). Overall, the stunning photomagnetic behavior of **1** might be related to the improved flexibility of the CN-bridged framework after H_2O removal which enables the coordination sphere reorganization including the photo-dissociation of the non-bridging cyanide ligand.

CONCLUSIONS

Our continuous study in the field of photomagnetic compounds has led to the unprecedented observation of a record high photo-induced magnetic ordering temperature of 93 K and a photo-induced magnetic hysteresis loop at 90 K in a $[W^{IV}(CN)_8]$-based 3-D coordination framework $\{[Mn^{II}(imidazole)]_2[W^{IV}(CN)_8]\}_n$ **1**. This unique photomagnetic behavior, which can be reversibly switched "on" and "off" (ex-situ) by the dehydration-rehydration process, clearly demonstrates that the application of multistable photomagnetic solids for the construction of novel photomagnetic devices is becoming feasible. Further efforts towards the construction of $[W^{IV}(CN)_8]$-based multifunctional photo-switchable magnets demonstrating even higher photo-induced magnetic ordering temperatures and better memory effects are in progress.

EXPERIMENTAL SECTION

All reagents were used as supplied from commercial sources (Sigma-Aldrich, Alfa Aesar). Potassium octacyanotungstate(IV) was synthesized according to a known literature method.[24] Samples for powder X-ray diffraction, IR and photomagnetic studies were prepared inside an argon-filled glovebox (H_2O < 0.5 ppm; Inert Technology).

Syntheses

$\{[Mn^{II}(imidazole)(H_2O)_2]_2[W^{IV}(CN)_8]\cdot 4H_2O\}_n$ (**1-8H$_2$O**) was obtained by mixing the water solution of 0.5 mmol (100 mg) $MnCl_2\cdot 4H_2O$ and 1.0 mmol (68 mg) imidazole in 10 mL water with

the water solution of 0.1 mmol (56 mg) of potassium octacyanotungstate(IV) dihydrate in 10 mL water. After 24 hours yellow column crystals were collected by decantation and dried shortly in air (typical yield: 30 mg, ca. 40 %). The purity was confirmed by elemental analysis. Anal. calcd for $C_{14}H_{24}Mn_2N_{12}O_8W$: C 21.48, H 3.09, N 21.50; found: C 21.68, H 2.76, N 21.47.

{[Mn^{II}(imidazole)]$_2$[W^{IV}(CN)$_8$]}$_n$ (**1**) was obtained by drying **1-8H$_2$O** over P_4O_{10} for 24 hours under vacuum (10^{-2} mbar) at room temperature. Anal. calcd for $C_{14}H_8Mn_2N_{12}W$: C 26.33, H 1.26, N 26.35; found: C 25.71, H 1.36, N 26.44.

Physical characterization

Elemental analysis was performed using the ELEMENTAR Vario Micro Cube CHNS analyzer. Solid state UV-Vis spectra were recorded using the PerkinElmer Lambda 35 UV/VIS spectrophotometer equipped with an integration sphere. For this measurement the sample suspended in paraffin oil was spread as a thin film between two fused quartz plates. IR spectra were recorded using Nicolet iN10 MX FT-IR microscope in the transmission mode and Linkam THMS350V temperature controlled stage. In the case of sorption reversibility IR measurements (**Figure S8**), **1-8H$_2$O** was dehydrated by heating to 80 °C in dry nitrogen atmosphere, while rehydration was performed by purging the sample chamber at room temperature with air at 95-100% RH.

Water sorption measurements

The water adsorption isotherm was measured by a Dynamic Vapor Sorption method using an SMS DVS Resolution apparatus in the 0-95% RH range at 298 K. The dehydration-rehydration cycles were performed at 298 K for sample held in 0% or 95% RH until a constant mass was reached.

Magnetic and photomagnetic measurements

Magnetic susceptibility measurements were performed using a Quantum Design MPMS-3 Evercool magnetometer in magnetic fields up to 7 Tesla. Samples for photomagnetic studies were ground to a fine powder and spread onto a colourless adhesive tape in form of a thin 0.05 mm layer (ca. 0.2 mg, 0.2 cm^2). In order to prevent **1-8H$_2$O** from dehydration in the magnetometer chamber, it was initially cooled down to 250 K and only then vacuum pumped. Irradiation was performed using a 450 nm laser diode (Thorlabs L450P1600MM). The power of the light was measured at the sample using Thorlabs Optical Power and Energy Meter PM100D. The experimental data were corrected for the diamagnetism of the sample and the sample holder. ZFC-FC measurements have been performed with 3 K·min^{-1} heating rate. $\chi T(T)$ was recorded with 2 K·min^{-1} heating rate..

Single crystal X-ray diffraction, structure solution and refinement

Single crystal X-ray diffraction experiments were performed using the Bruker D8 Quest Eco Photon50 CMOS diffractometer at 120 K (Mo Kα radiation, graphite monochromator). Absorption correction, data reduction and unit cell refinement were performed using SADABS and SAINT programs included in the Apex3 suite. The structure was solved using direct methods and refined anisotropically using weighted full-matrix least-squares on F^2.[25] H-atoms of the imidazole ligands were placed in the calculated positions and refined as riding on the parent atoms. H-atoms of water molecules were located from difference Fourier map and refined with their U_{iso} fixed at 1.2U_{iso} of the parent oxygen atoms. The O-H distances were fixed at 0.95 Å and the H-O-H angles were restrained using DANG command in SHELXL. Structural diagrams were prepared using Mercury CSD 3.9.[26] CCDC 1814690 contains the supplementary crystallographic data for **1-8H$_2$O**. These data can be obtained free of charge from The Cambridge Crystallographic Data Centre via www.ccdc.cam.ac.uk/data_request/cif.

Powder X-ray diffraction, structure solution and refinement

PANalytical X'Pert Pro diffractometer with CuKα radiation (λ = 1.54178 Å) was used to collect all X-Ray powder diffraction data. The measurements were performed at room temperature in the 3-50° 2θ angle range. The crystal structure of **1** was determined based on the structural model of the {[Mn^{II}(imH)]$_2$[Nb^{IV}(CN)$_8$]}$_n$ analogue reported previously.[14] The unit cell was found in a triclinic system with the following parameters: a = 9.9810(5) Å, b = 10.8463(5) Å, c = 9.8571(5) Å, α = 103.871(3)°, β =103.223(3)°, γ = 95.421(4)°, V = 995.85(9) Å^3 (space group *P-1*) using PROSZKI package.[27] The parameters were obtained by refining the unit cell of {[Mn^{II}(imH)]$_2$[Nb^{IV}(CN)$_8$]}$_n$. Direct implementation of the previous model for the structure refinement was impossible and the solution had to be determined from the beginning. To solve the structure, positions of one [W^{IV}(CN)$_8$]$^{4-}$ and two [Mn(imidazole)]$^{2+}$ moieties were optimized based on the direct-space method implemented in the *FOX* software.[28] Rietveld refinement of the model was carried out using JANA2000 software.[29] The final agreement factors are R_p = 0.0322 and R_{wp} = 0.0412. Due to the large number of light atoms in the model, which led to the instability of the refinement, only rigid-body refinement of the above presented moieties was performed. This procedure generates noticeably larger errors in some bond lengths and angles as compared to the traditionally refined structures. However, the agreement between the observed and calculated patterns (**Figure S4**) suggests that the framework of the structure was obtained with acceptable precision. CCDC 1859185 contains the supplementary crystallographic data for **1**. These data can be obtained free of charge from The Cambridge Crystallographic Data Centre via www.ccdc.cam.ac.uk/data_request/cif.

ASSOCIATED CONTENT

Supporting Information

The Supporting Information is available free of charge on the ACS Publications website. Additional structural diagrams, IR spectra, magnetic plots and schemes

AUTHOR INFORMATION

Corresponding Author

dawid.pinkowicz@uj.edu.pl

Notes

The authors declare no competing financial interests.

ACKNOWLEDGMENT

This work was financed by the Polish National Science Centre within the Sonata Bis 6 (2016/22/E/ST5/00055) and the Opus 8 (2014/15/B/ST5/04465) research projects. MM gratefully acknowledges the Polish Ministry of Science and Higher Education for the financial support within the „Diamond Grant“ project (0192/DIA/2017/46).

REFERENCES

(1) a) J.-M. Lehn, *Angew. Chem. Int. Ed.*, **2015**, *54*, 3276; b) J.-F. Lutz, J.-M. Lehn, E. W. Meijer, K. Matyjaszewski, *Nat. Rev. Mater.* **2016**, *1*, 16024

(2) a) B. Sieklucka, D. Pinkowicz, Molecular Magnetic Materials: Concepts and Applications, Wiley-VCH, Weinheim, **2017**; b) C. Mathonière, H. Tokoro, S.-I. Ohkoshi, **2016**. Molecular Photomagnets. In Molecular Magnetic Materials (eds B. Sieklucka and D. Pinkowicz); c) L. Ouahab, Ed., Multifunctional Molecular Materials, Pan Stanford Publishing Pte. Ltd., Singapore, **2013**; d) D. Gatteschi, R. Sessoli, R. Villain, *Molecular Nanomagnets*, Oxford University Press, New York **2006**

(3) a) S. Manz, M. Matsubara, T. Lottermoser, J. Büchi, A. Iyama, T. Kimura, D. Meier, M. Fiebig, *Nat. Photonics*, **2016**, *10*, 653-656; b) B. Kundys, M. Viret, D. Colson, D. O. Kundys, *Nat. Mater.*, **2010**, *9*, 803-805; c) N. Kanda, T. Higuchi, H. Shimizu, K. Konishi, K. Yoshioka, M. Kuwata-Gonokami, *Nat. Commun.*, **2011**, *2*, 362.

(4) a) O. M. Yaghi, M. O'Keeffe, N. W. Ockwig, H. K. Chae, M. Eddaoudi, *Nature*, **2003**, *423*, 705-714; b) M. J. Kalmutzki, C. S. Diercks, O. M. Yaghi, *Adv. Mater.*, **2018**, *30*, 1704304; c) B. Li, H.-M. Wen, Y. Cui, W. Zhou, G. Qian, B. Chen, *Adv. Mater.*, **2016**, *28*, 8819 d) S. A. Chavan, J. Larionova, O. Kahn, J. B. Yakhmi, *Philos. Mag. B*, **1998**, *77*, 1657; e) P. Dechambenoit, J. R. Long, *Chem. Soc. Rev.*, **2011**, *40*, 3249 f) J. Milon, M.-C. Daniel, A. Kaiba, P. Guionneau, S. Brandes, J.-P. Sutter, *J. Am. Chem. Soc.*, **2007**, *129*, 13872; g) D. Pinkowicz, R. Podgajny, B. Gaweł, W. Nitek, W. Łasocha, M. Oszajca, M. Czapla, M. Makarewicz, M. Bałanda, B. Sieklucka, *Angew. Chem. Int. Ed.*, **2011**, *50*, 3973.

(5) a) C. Mathonière, R. Podgajny, P. Guionneau, C. Labrugere, B. Sieklucka, *Chem. Mater.*, **2005**, *17*, 442; b) A. Bleuzen, V. Marvaud, C. Mathonière, B. Sieklucka, M. Verdaguer, *Inorg. Chem.*, **2009**, *48*, 3453

(6) a) M. Nihei, Y. Okamoto, Y. Sekine, N. Hoshino, T. Shiga, I. P.-C. Liu, H. Oshio, *Angew. Chem. Int. Ed.*, **2012**, *51*, 6361; b) N. Hoshino, F. Iijima, G. N. Newton, N. Yoshida, T. Shiga, H. Nojiri, A. Nakao, R. Kumai, Y. Murakami, H. Oshio, *Nat. Chem.* **2012**, *4*, 921; c) C. Mathonière, H.-J. Lin, D. Siretanu, R. Clérac, J. M. Smith, *J. Am. Chem. Soc.* **2013**, *135*, 19083

(7) a) Y.-S. Meng, O. Sato, T. Liu *Angew. Chem. Int. Ed.* **2018**, *57*, 12216-12226; b) C. Mathonière *Eur. J. Inorg. Chem.* **2018**, 248-258; c) Y. Arimoto, S.-i. Ohkoshi, Z. J. Zhong, H. Seino, Y. Mizobe, K. Hashimoto, *J. Am. Chem. Soc.* **2003**, *125*, 9240; d) S.-i. Ohkoshi, S. Ikeda, T. Hozumi, T. Kashiwagi, K. Hashimoto, *J. Am. Chem. Soc.* **2006**, *128*, 5320; e) N. Ozaki, H. Tokoro, Y. Hamada, A. Namai, T. Matsuda, S. Kaneko, S.-i. Ohkoshi, *Adv. Funct. Mater.*, **2012**, *22*, 2089;

(8) a) S. Decurtins, P. Gütlich, C. P. Köhler, H. Spiering, *Chem. Phys. Lett.*, **1984**, *105*, 1; b) X. Feng, C. Mathonière, l-R. Jeon, M. Rouzières, A. Ozarowski, M. L. Aubrey, M. I. Gonzalez, R. Clérac, J. R. Long, *J. Am. Chem. Soc.*, **2013**, *135*, 15880; c) J.-F. Létard, J. Mater. Chem., 2006, 16, 2550; d) G. Chastanet, C. Desplanches, C. Baldé, P. Rosa, M. Marchivie, P. Guinneau *Chem. Sq.* **2018**, *2*, 2

(9) a) G. Poneti, M. Mannini, B. Cortigiani, L. Poggini, L. Sorace, E. Otero, P. Sainctavit, R. Sessoli, A. Dei, *Inorg. Chem.*, **2013**, *52*, 11798; b) O. Drath, R. W. Gable, B. Moubaraki, K. S. Murray, G. Poneti, L. Sorace, C. Boskovic, *Inorg. Chem.*, **2016**, *55*, 4141; c) O. Drath, C. Boskovic, Coord. Chem. Rev., **2017**, *375*, 256-266.

(10) a) S. Brossard, F. Volatron, L. Lisnard, M.-A. Arrio, L. Catala, C. Mathonière, T. Mallah, C. Cartier dit Moulin, A. Rogalev, F. Wilhelm, A. Smekhova, P. Sainctavit, *J. Am. Chem. Soc.*, **2012**, *134*, 222; b) N. Bridonneau, J. Long, J.-L. Cantin, J. von Bardeleben, S. Pillet, E.-E. Bendeif, D. Aravena, E. Ruiz, V. Marvaud, *Chem. Commun.*, **2015**, *51*, 8229; c) T. Korzeniak, R. Jankowski, M. Kozieł, D. Pinkowicz, B. Sieklucka, *Inorg. Chem.*, **2017**, *56*, 12914

(11) M. Magott, O. Stefańczyk, B. Sieklucka, D. Pinkowicz, *Angew. Chem. Int. Ed.*, **2017**, *56*, 13283

(12) a) L. Shen, Y. Zhang, J. Uiu, *J. Coord. Chem.*, **2006**, *59*, 629; b) D. Pinkowicz, R. Podgajny, W. Nitek, M. Makarewicz, M. Czapla, M. Mihalik, M. Bałanda, B. Sieklucka, *Inorg. Chim. Acta*, **2008**, *361*, 3957

(13) a) M. Llunell, D. Casanova, J. Cirera, P. Alemany, S. Alvarez, SHAPE v. 2.1, **2013**, University of Barcelona: Barcelona, Spain. b) D. Casanova, M. Llunell, P. Alemany, S. Alvarez, *Chem. Eur. J.*, **2005**, *11*, 1479

(14) D. Pinkowicz, R. Podgajny, M. Bałanda, M. Makarewicz, B. Gaweł, W. Łasocha, B. Sieklucka, *Inorg. Chem.*, **2008**, *47*, 9745

(15) P. Crewdson, S. Gambarotta, G. P. A. Yap, L. K. Thompson, *Inorg. Chem.*, **2003**, *42*, 8579

(16) a) H. Kim, S. Yang, S. R. Rao, S. Narayanan, E. A. Kapustin, H. Furukawa, A. S. Umans, O. M. Yaghi, E. N. Wang, *Science*, **2017**, *356*, 430-434; b) H. Furukawa, F. Gándara, Y.-B. Zhang, J. Jiang, W. L. Queen, M. R. Hudson, O. M. Yaghi, *J. Am. Chem. Soc.*, **2014**, *136*, 4369; c) A. J. Rieth, S. Yang, E. N. Wang, M. Dinča, *ACS Cent. Sci.*, **2017**, *3*, 668

(17) J. S. Beck, J. C. Vartuli, W. J. Roth, M. E. Leonowicz, C. T. Kresge, K. D. Schmitt, C. T. W. Chu, D. H. Olson, E. W. Sheppard, S. B. McCullen, J. B. Higgins, J. L. Schlenker, *J. Am. Chem. Soc.*, **1992**, *114*, 10834

(18) J. H. Cavka, S. Jakobsen, U. Olsbye, N. Guillou, C. Lamberti, S. Bordiga, K. P. Lillerud, *J. Am. Chem. Soc.*, **2008**, *130*, 13850

(19) H. Reinsch, M. A. van der Veen, B. Gil, B. Marszałek, T. Verbiest, D. de Vos, N. Stock, *Chem. Mater.*, **2013**, *25*, 17

(20) N. F. Chilton, R. P. Anderson, L. D. Turner, A. Soncini and K. S. Murray *J. Comput. Chem.* **2013**, *34*, 1164-1175

(21) a) B. Sieklucka, *Prog. React. Kinet. Mec.*, **1999**, *24*, 165; b) J. Szklarzewicz, A. Samotus, O. Traverso, S. Sostero, *Polyhedron*, **1994**, *13*, 1755 c) J. Szklarzewicz, D. Matoga, A. Niezgoda, D. Yoshioka, M. Mikuriya, *Inorg. Chem.*, **2007**, 46, 9531

(22) a) M.-A. Carvajal, M. Reguero, C. de Graaf, *Chem. Commun.*, **2010**, *46*, 5737 b) M.-A. Carvajal, R. Caballol, C. de Graaf, *Dalton. Trans.*, **2011**, *40*, 7295

(23) F. J. Birk, D. Pinkowicz, K. R. Dunbar, *Angew. Chem. Int. Ed.*, **2016**, *55*, 11368

(24) D. Matoga, J. Szklarzewicz, M. Mikuriya, *Inorg. Chem.*, **2006**, *45*, 7100

(25) a) G. Sheldrick, *Acta Crystallogr., Sect. A: Found. Crystallogr.*, **2008**, *64*, 112 b) G. Sheldrick, *Acta Crystallogr., Sect. C: Struct. Chem.*, **2015**, *71*, 3 c) O. V. Dolomanov, L. J. Bourhis, R. J. Gildea, J. A. K. Howard, H. Puschmann, *J. Appl. Cryst.*, **2009**, *42*, 339

(26) C. F. Macrae, I. J. Bruno, J. A. Chisholm, P. R. Edgington, P. McCabe, E. Pidcock, L. Rodriguez-Monge, R. Taylor, J. van de Streek, P. A. Wood, *J. Appl. Cryst.*, **2008**, *41*, 466

(27) W. Łasocha, K. Lewiński, *J. Appl. Crystallogr.* **1994**, *27*, 437

(28) V. Favre-Nicolin, R. Cerny, *J. Appl. Cryst.* **2002**, *35*, 734-743

(29) V. Petricek, M. Dusek, L. Palatinus, *Jana2000, The crystallographic computing system*, Institute of Physics, Praha, Czech Republic, **2000**.

TOC graphic